Effect of Sealing Air on Oil Droplet and Oil Film Motions in Bearing Chamber

SUN Heng-chao, CHEN Guo-ding, YOU Hao, CHEN Jun-yu
School of Mechanical Engineering, Northwestern Polytechnical University, Xi´an 710072, P. R. China

Abstract: Bearing chamber is one of important components that support aero-engine rotors and research on oil droplet and oil film motions is an important part of bearing chamber lubrication and heat transfer design. Considering the pressure of sealing air is an important operating condition that affects the oil droplet and oil film motions, the effect of sealing air pressure on airflow in bearing chamber is investigated in this paper firstly; and then based on the air velocity and air/wall shear force, the oil droplet moving in core air, deposition of oil droplet impact on wall as well as velocity and thickness of oil film are analyzed secondly; the effect of sealing air pressure on oil droplet velocity and trajectory, deposition mass and momentum, as well as oil film velocity and thickness is discussed. The work presented in this paper is conducive to expose the oil/air two phase lubrication mechanism and has certain reference value to guide design of secondary air/oil system.

Key words: aero-engine; bearing chamber; sealing air; two phase flow; droplet; oil film; calculation; drag coefficient; film thickness; model; trajectory; velocity

1 Introduction

Bearing chamber is important component of aero-engine and gives a guarantee of roller bearings and rotors running reliably, in bearing chamber the high rotational bearing rolling elements push the oil, which flows from under race lubrication system, change to oil droplets, the discrete oil droplets are ejected to static outer wall and transform to oil film. To prevent oil leakage from bearing chamber, seals have to be pressured by air. The air mixing with the oil generates extremely complex two phase flow. The lubrication and heat transfer design of bearing chamber require a sufficient understanding and correct analysis into oil/air two phase flow, and so that has attracted extensive interest.

Owing to that have significant influence on the lubrication and heat transfer characteristics of bearing chamber, the oil droplet and oil film motions become the most important research aspects of oil/air two phase flow in bearing chamber. Lee, et al. [1] calculated the airflow in bearing chamber with numerical method and compared the air velocity with the available experimental data that was measured by Particle Image Velocimetry (PIV) technology. Glahn, et al. [2] measured the size and velocity of oil droplets in bearing chamber with Phase Doppler Particle Analyzer (PDPA), and with the help of numerical method the velocity and trajectory of oil droplet were computed, the effect of rotational rate on droplet velocity was discussed. Gorse, et al. [3] measured the oil film thickness on some circumferential location of chamber housing using capacitive sensors, combining with the consumption about oil film velocity profile, the oil film thicknesses on the other locations were calculated. Farrall, et al. [4] put forward a two-dimension oil droplet movement analysis model, the effect of oil droplet initial conditions on oil droplet movement characteristic was investigated. Wang, et al. [5] analyzed the airflow in the chamber-rotating structure that was similar to bearing chamber, effects of some oper-

Received 04 August 2013
This paper is supported by the Natural Science Foundation of China under Grant No. 51275411

ating and geometrical parameters on airflow were discussed. Chen, et al. [6] calculated the airflow field in a typical aero-engine bearing chamber with the commercial computational fluid dynamics package taking into consideration the airflow sate equations. Chen, et al. [7~9] introduced the oil droplet size (mass) distribution function, the droplet mass deposition and momentum transfer were investigated and the researches of oil droplet movement, droplet impingement and deposition as well as the flow behavior of oil film were integrated.

The above-mentioned works have several limitations. The research on oil droplet and film motions didn't investigate the effect of sealing air pressure or mass flow rate on oil droplet and oil film motions, and the reason is that the effect of sealing air pressure or mass flow rate on oil droplet and film motions is indirect and the effect is realized by the airflow affecting on the drag force applied to oil droplet and shear force applied to oil film, however, the existing research, that focus on oil droplet and oil film motions, is weakly developed about effect of air pressure on airflow because the calculation workload is too much and the experiments are expensive. In the present paper, correction factors reflect sealing air pressure influence on airflow in bearing chamber have been proposed and the effect of sealing air on airflow has been discussed with the help of correction factors, correction relationship between sealing air pressure with air tangential velocity and air/wall shear force. On the basic of airflow investigation, the oil droplet motion in core air, deposition of oil droplet impacts on wall as well as velocity and configuration of oil film have been analyzed, the effect of sealing air pressure on oil droplet and oil film motions has been obtained. The current work, not only improves the integrality of studies into oil/air two phase flow in bearing chamber, but also has certain reference value to guide design secondary air/oil system.

2 Configuration of bearing chamber and related parameters

A typical configuration of aero-engine bearing chamber is shown schematically in Figure 1. The main configuration parameters, unless otherwise stated, are as follows: radius of rotating shaft $r_s = 75$ mm, width of bearing chamber $b = 105$ mm, height of bearing chamber $h = 75$ mm, diameters of vent and scavenge $d_v = 16$ mm.

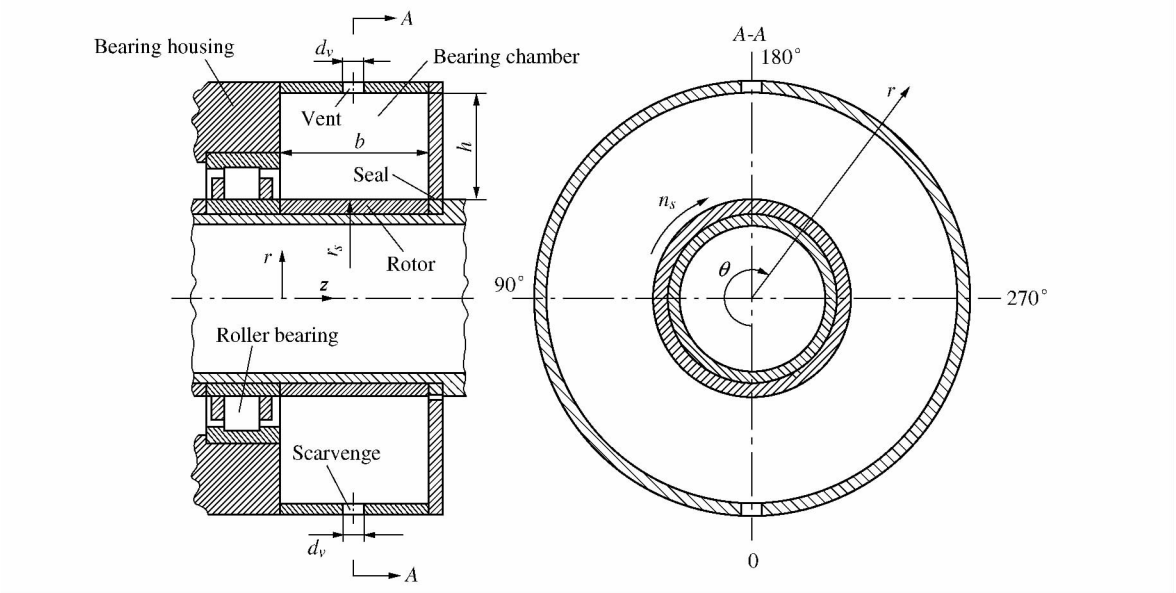

Figure 1 Schematic of aero-engine bearing chamber

3 Fitting formulas of airflow velocity and air/wall shear force

Because of the scavenge of bearing chamber is covered by the oil when it is working and the oil film thickness is negligible compared with size of the chamber, the airflow analysis in bearing chamber does not involve the function of scavenge.

Firstly, without considering inlet of sealing air, under chamber heights $h = 60$ mm, 75 mm, 90 mm and 105 mm combining rotational rates $n_s = 6\,000$ r/min, 9 000 r/min, 12 000 r/min and 15 000 r/min, the airflow fields in bearing chamber are solved by commercial computational fluid dynamics software, physical parameters of air are as follows: air dynamic viscosity $\mu_g = 1.789 \times 10^{-5}$ kg/(m·s) and density $\rho_g = 1.225$ kg/m^3. The distributions of air tangential velocity along radial direction and air/wall shear force along axial direction are obtained with fitting formulas such as the polynomials shown by Equation (1) and Equation (2) respectively.

$$u_{gt} = a_0 + a_1 r^* + a_2 r^{*2} + a_3 r^{*3} + a_4 r^{*4} + a_5 r^{*5} \quad (1)$$

$$\tau_g = b_0 + b_1 z + b_2 z^2 \quad (2)$$

Where u_{gt} denotes air tangential velocity in bearing chamber; r^* is no dimensional radial coordinate and $r^* = (r - r_s)/h$, r is radial coordinate of cylinder coordinate system shown as Figure 1; τ_g is air/wall shear force; a_0 et al are coefficients of polynomials and their values are shown as Table 1.

Table 1 Coefficients of fitting formulas about air velocity and air/wall shear force

No.	Chamber height h/mm	Rotational rate n_s/(r·min^{-1})	a_0	a_1	a_2	a_3	a_4	a_5	b_0	b_1	b_2
1	60	6 000	25.19	−266.4	1 306	−2 817	2 739	−983.4	0.228	2.45	−36.06
2	60	9 000	39.62	−231.9	986.4	−2 095	2 073	−764.0	0.267	25.58	−227.0
3	60	12 000	47.71	−437.1	2 178	−4 727	4 611	−1 662	0.410	31.36	−282.3
4	60	15 000	60.31	−560.5	2 778	−6 050	5 935	−2 152	1.128	19.48	−231.1
5	75	6 000	26.84	−220.4	1 118	−2 489	2 471	−902.9	0.162 2	3.90	−34.31
6	75	9 000	41.32	−370.6	1 732	−3 622	3 445	−1 219	0.212 6	19.75	−174.2
7	75	12 000	46.29	−447.3	2 253	−4 896	4 750	−1 697	0.233 6	28.3	−238.7
8	75	15 000	57.06	−564.9	2 823	−6 115	5 927	−2 117	0.365 7	36.26	−324.6
9	90	6 000	23.75	−274.4	1 363	−2 972	2 910	−1 049	0.108 1	1.991	−24.85
10	90	9 000	35.37	−397.6	1 950	−4 208	4 091	−1 468	0.260 6	3.894	−51.32
11	90	12 000	46.05	−516.4	2 533	−5 484	5 353	−1 828	0.451 1	5.638	−80.61
12	90	15 000	55.50	−554.3	2 783	−6 078	5 929	−2 126	0.341 7	27.08	−243.4
13	105	6 000	26.30	−192.0	956.2	−2 180	2 232	−837.9	0.155 0	2.224	−18.19
14	105	9 000	35.20	−324.3	1 626	−3 599	3 578	−1 311	0.271 5	4.902	−46.09
15	105	12 000	49.24	−544.8	2 684	−5 817	5 679	−2 045	0.425 7	5.97	−73.05
16	105	15 000	57.78	−592.2	2 885	−6 211	6 038	−2 172	0.625 5	9.598	−106.7

In order to build the relationship between correction factors, which reflect sealing air pressure influence on airflow tangential velocity and air/wall shear force in bearing chamber, with sealing air pressures, under chamber heights $h = 60$ mm, 105 mm and rotational rates $n_s = 6\ 000$ r/min and 15 000 r/min combining sealing air pressures $p_{g,\mathrm{in}} = 10$ kPa, 20 kPa, 30 kPa, 40 kPa and 50 kPa, the airflow fields in bearing chamber are solved again, comparing the airflow tangential velocity and air/wall shear force under various air inlet pressures to that of without considering inlet of sealing air, relationships between correction factors with sealing air pressure are obtained.

$$C = 0.754\ 29 - 0.004\ 1p_{g,\mathrm{in}} - 2.756\ 91 \times 10^{-5} p_{g,\mathrm{in}}^2 \tag{3}$$

$$J = 0.690\ 48 - 0.021\ 49p_{g,\mathrm{in}} + 1.279\ 29 \times 10^{-4} p_{g,\mathrm{in}}^2 \tag{4}$$

With the correction factors and Equations (1) ~ (2), the airflow tangential velocity and air/wall shear force with considering of sealing air pressure are shown as follows

$$u_{gtp} = C^* \ u_{gt} \tag{5}$$

$$\tau_{gp} = J^* \ \tau_g \tag{6}$$

For the other chamber heights and rotational rates except above mentioned, the airflow tangential velocity and air/wall shear force can be calculated by linear interpolation.

4 Calculation models of oil droplet and oil film motions

4.1 Oil droplet motion in airflow

The oil droplet moving in bearing chamber is primarily affected by air resistance and in the cylindrical coordinates shown in Figure 1, the kinematic equations of oil droplet in tangent, radial and axial direction can be deduced from theorem of momentum as follows:

$$\begin{cases} m_d \dfrac{\mathrm{d}u_{dt}}{\mathrm{d}t} = \dfrac{1}{2} C_d S \rho_g \mid \boldsymbol{u}_g - \boldsymbol{u}_d \mid (u_{gtp} - u_{dt}) \\ m_d \dfrac{\mathrm{d}u_{dr}}{\mathrm{d}t} = \dfrac{1}{2} C_d S \rho_g \mid \boldsymbol{u}_g - \boldsymbol{u}_d \mid (u_{grp} - u_{dr}) \\ m_d \dfrac{\mathrm{d}u_{dz}}{\mathrm{d}t} = \dfrac{1}{2} C_d S \rho_g \mid \boldsymbol{u}_g - \boldsymbol{u}_d \mid (u_{gzp} - u_{dz}) \end{cases} \tag{7}$$

Where m_d denotes mass of oil droplet; C_d is drag coefficient; S is windward area of droplet; $\boldsymbol{u}_g$ and $\boldsymbol{u}_d$ are velocity vectors of air and oil droplet respectively; u_{gtp}、u_{grp} and u_{gzp} are tangent, radial and axial velocities of air respectively; u_{dt}、u_{dr} and u_{dz} are tangent, radial and axial velocities of oil droplet respectively.

The difference equation of oil droplet motion can be deduced from Equation (7) and is shown as follows:

$$\begin{cases} u_{dt1}^i = u_{dt0}^i + \dfrac{3}{8} C_d \dfrac{\rho_g}{\rho_d} \dfrac{\mid \boldsymbol{u}_{g0}^i - \boldsymbol{u}_{d0}^i \mid}{r_d} (u_{gt0}^i - u_{dt0}^i) \Delta t \\ u_{dr1}^i = u_{dr0}^i + \dfrac{3}{8} C_d \dfrac{\rho_g}{\rho_d} \dfrac{\mid \boldsymbol{u}_{g0}^i - \boldsymbol{u}_{d0}^i \mid}{r_d} (u_{gr0}^i - u_{dr0}^i) \Delta t \\ u_{dz1}^i = u_{dz0}^i + \dfrac{3}{8} C_d \dfrac{\rho_g}{\rho_d} \dfrac{\mid \boldsymbol{u}_{g0}^i - \boldsymbol{u}_{d0}^i \mid}{r_d} (u_{gz0}^i - u_{dz0}^i) \Delta t \end{cases} \tag{8}$$

Where i means the ith time step whose initial and end times are represented with subscript "0" and "1" respectively, Δt is the time span of time step, r_d is the radius of droplet. The tangent, radial and axial displacements ($\mathrm{d}s$, $\mathrm{d}r$ and $\mathrm{d}z$) as well as angular displacement $\mathrm{d}\theta$ of oil droplet in the ith time step can be calculated with

$$\begin{cases} \mathrm{d}s = \dfrac{u_{dr0}^i + u_{dt1}^i}{2} \Delta t \\ \mathrm{d}r = \dfrac{u_{dr0}^i + u_{dr1}^i}{2} \Delta t \\ \mathrm{d}z = \dfrac{u_{dz0}^i + u_{dz1}^i}{2} \Delta t \end{cases} \tag{9}$$

$$\mathrm{d}\theta = \arctan \frac{\mathrm{d}s}{r_0^i + \mathrm{d}r} \tag{10}$$

With the velocity and position of the oil droplet at end time of ith time step (the same as those at initial time of $(i+1)$th time step), the calculation about the $(i+1)$th time step can be conducted. In this way the trajectories and velocities of oil droplets in bearing chamber and the moving state of oil droplets before impacting on the chamber wall can be obtained under the initial conditions after the oil droplets shedding from bearing.

4.2 Oil droplet mass distribution

The oil droplets shed from bearing have various diameters; the droplet size distribution can be transformed from mass distribution for spherical droplet. The mass distribution of oil droplets in bearing chamber can be expressed by Rossin-Rammler (R-R) function:

$$f_m = S\left[\frac{d_d^{S-1}}{\bar{d}^S}\right]\mathrm{e}^{-\left(\frac{d_d}{\bar{d}}\right)^S} \tag{11}$$

Where d_d is the diameter of oil droplet; $\bar{d}$ is the characteristic diameter of mass distribution and has a physical meaning that the ratio of summarized mass of oil droplets whose diameters are larger than $\bar{d}$ to the total mass of all oil droplets is 36.8%; S is the spread parameters of the distribution. The values of $\bar{d}$ and S have a close relationship with the operating parameters of bearing chamber and their expressions are presented in Reference [9].

4.3 Deposited mass and momentum of oil droplets

Moving droplets will be resisted by different air resistant effects due to their diameter difference, and lead to the different velocities and momentum of oil droplets when impingement. Two impingement situations of oil droplets have been investigated including of the oil droplets are direct deposition and the break-up oil droplets producing many secondary droplets. The mass of direct depositing droplets transfers to oil film, but only tangent momentum component of direct depositing droplets transfers to oil film because radial momentum component loses in the process of impingement. Deposited mass and tangent momentum component of break-up oil droplets transfer to oil film. The splashed part of break-up oil droplet forms some smaller secondary droplets in which some larger secondary droplets may be deposited again and the other smaller are air suspended and discharged from the vent port. The velocity of secondary droplets is disordered when deposited, therefore no momentum of secondary droplets transfer to oil film because their momentum neutralizes each other to zero. The film mass transferred from oil droplets is made up of the mass of direct deposited droplets, the deposited mass of break-up oil droplets and the subsequent deposited mass of secondary droplets. The film momentum is made up of the tangent momentum of direct deposited droplets and that of deposited part of break-up oil droplets.

The diameter range of oil droplets $[d_{d\min}, d_{d\max}]$ is divided into n equal internals and the impacting state is estimated for the oil droplets whose diameters are in the interval $[d_{di}, d_{di+1}]$. The deposited mass per unit time

$$m_c = \rho_d L\sum_{i=1}^{n}\eta_i\int_{d_{di}}^{d_{di+1}} S\left[\frac{d_d^{S-1}}{\bar{d}^S}\right]\mathrm{e}^{-\left(\frac{d_d}{\bar{d}}\right)^S}\mathrm{d}d_d \tag{12}$$

Where L is the oil mass flow rate supplied to bearing chamber, η_i is the mass deposition efficiency of oil droplets in relevant interval and is expressed as Reference [9], and the subsequent deposited mass is involved for the secondary oil droplets circumstance. The subsequent depositing mass of secondary oil droplets m_{sdc} is expressed as

$$m_{sdc} = \frac{1}{6}\pi\rho_d N\int_{0.000\,025}^{d_{s\max}} d_s^3 g_2(d_s)\,\mathrm{d}d_s \tag{13}$$

Where N is the number of secondary oil droplets, d_s is the diameter of secondary oil droplet, $d_{s\max}$ is the maximal diameter of secondary oil droplet, $g_2(d_s)$ is the total distribution density of secondary oil droplets corresponding to different diameters and is expressed as Reference [4].

In the same way, the momentum of oil film transferred from deposited droplets per unit time p_c is expressed as

$$p_c = \rho_d L u_{d0}\sum_{i=1}^{n}\lambda_i\int_{d_{di}}^{d_{di+1}} S\left[\frac{d_d^{S-1}}{\bar{d}^S}\right]\mathrm{e}^{-\left(\frac{d_d}{\bar{d}}\right)^S}\mathrm{d}d_d \tag{14}$$

where λ is momentum transfer efficiency of oil droplets and is expressed as Reference [2].

4.4 Oil film thickness and velocity

Since the oil film is thin compared to the size of bearing chamber, the oil/air interfacial shear stress along the chamber circumference is treated as a constant. The pressure difference and acceleration inside oil film are neglected. The oil film has no movement in axial direction owing to the circumference movement of rotating elements. Take the oil film section at θ position in the bearing chamber as the investigation subject. At high rotational rate ($n \geqslant 12\ 000$ r/min), the momentum of oil film can overcome the gravity and wall shear force, and drags oil film flow along the chamber wall. The oil film force balance can be described by Figure 2. At low rotational rate ($n \leqslant 9\ 000$ r/min), the motion of oil film at chamber down side is in the direction of gravity force, so that the oil film force balance can still be described by Figure 2. But the motion of oil film at chamber rising side is opposite to the bearing rotational direction because of small oil/air interfacial shear force and oil film momentum. The oil film force balance is presented in Figure 3.

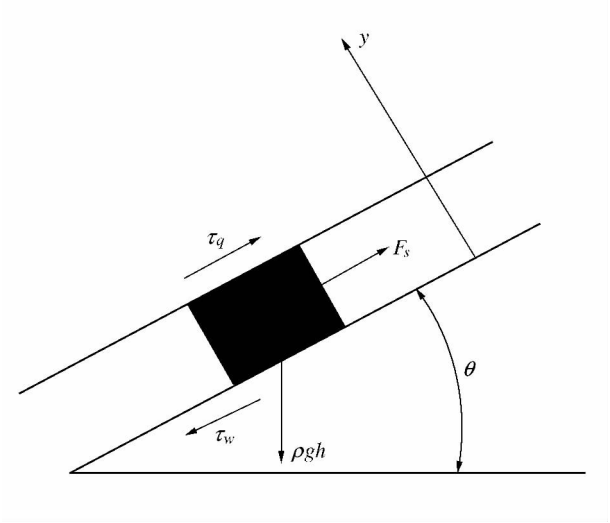

Figure 2 Force balance of oil film at hignt rotational rate

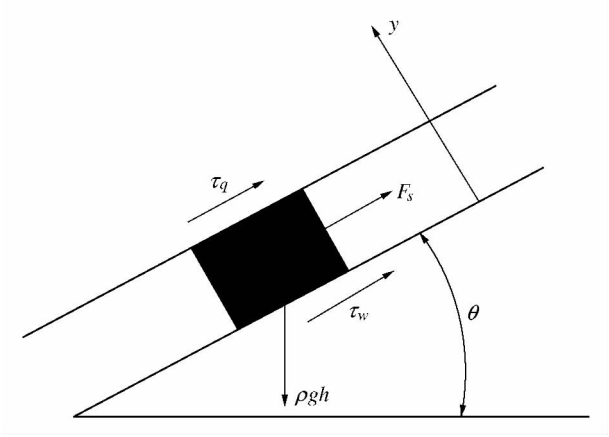

Figure 3 Force balance of oil film at low rotational rate

In Figures 2 ~ 3, F_s is equivalent force and can be calculated by the momentum of deposited oil film per unit area; τ_q is the interface shear force between air and oil film and can be replaced by the average value of τ_{qp} in axial direction; τ_w can be deduced with Newton's Law and the assumption that the oil film velocity along thickness direction is distributed in parabola form. The force equilibrium equations of oil film section in tangent direction at high and low rotational speed are presented as follows respectively

$$\frac{p_c}{s} + \bar{\tau}_q = 3\mu \frac{\bar{u}}{h} + \rho_d g h \sin\theta \qquad (15)$$

$$\begin{cases} \dfrac{p_c}{s} + \bar{\tau}_q + 3\mu \dfrac{\bar{u}}{h} = \rho_d g h \sin\theta & 0 \leqslant \theta \leqslant 180° \\ \dfrac{p_c}{s} + \bar{\tau}_q - 3\mu \dfrac{\bar{u}}{h} = \rho_d g h \sin\theta & 180° < \theta \leqslant 360° \end{cases} \qquad (16)$$

Where s is internal surface area of bearing chamber.

The oil droplets shed from the bearing inner ring eject to the chamber wall uniformly and form oil film. The film driven by oil/air interfacial shear force and gravity flows along the chamber wall. The film is thin at upper region and thick at lower region of the flow. This implicates that the oil film volume flow varies at different chamber wall's circumferential location. By using mass conservation law, the oil film mean velocity distribution under high rotational speed condition is defined as

$$\begin{cases} \bar{u}(\theta) = \dfrac{m_c}{\rho_d hb} \cdot \dfrac{\theta}{360^\circ} & 0 \leqslant \theta \leqslant 180^\circ \\ \bar{u}(\theta) = \dfrac{m_c}{\rho_d hb} \cdot \dfrac{\theta - 180^\circ}{360^\circ} & 180^\circ < \theta \leqslant 360^\circ \end{cases} \tag{17}$$

The oil film mean velocity distribution under low rotational speed condition is defined as

$$\begin{cases} \bar{u}(\theta) = \dfrac{m_c}{\rho_d hb} \cdot \dfrac{180 - \theta}{360} & 0 \leqslant \theta \leqslant 180^\circ \\ \bar{u}(\theta) = \dfrac{m_c}{\rho_d hb} \cdot \dfrac{\theta - 180}{360} & 180^\circ < \theta \leqslant 360^\circ \end{cases} \tag{18}$$

The oil film thickness distribution $h(\theta)$ and the mean velocity distribution $\bar{u}(\theta)$ under high and low rotational speed conditions are obtained by the simultaneous solutions of Equation (15) and Equation (17) as well as Equation (16) and Equation (18) respectively.

5 Results and discussion

Based on the airflow tangential velocity and air/wall shear force, the effect of sealing air pressure on oil droplet motion, oil droplet/wall impingement deposition and oil film flow is investigated, the parameters in the analysis, unless otherwise specified, are as follows: density of oil $\rho_d = 953$ kg/m^3, dynamic viscosity of oil $\mu_d = 0.0095$ Pa · s, rotational rate of rotor $n_s = 10\,500$ r/min, width of bearing chamber $b =$ 105 mm, height of bearing chamber $h = 90$ mm, radius of rotor $r_s = 75$ mm, mass flow rate of oil $L =$ 39.75 g/s, axial angel of oil droplet shedding from bearing $\beta = 15^\circ$.

5.1 Influence on oil droplet velocity and trajectory

Figure 4 shows the effect of sealing air pressure on oil droplet velocity, whose diameter is 80 μm. It is noted from Figure 4 that, when the droplet is moving close to the chamber wall ($r \geqslant 150$ mm), the effect of sealing air pressure on its velocity becomes apparent. The reason can be explained as follows: the effect scope of sealing air pressure on airflow velocity is near the inlet of air, namely the seal, and the inlet of air is farm away from the region of droplet motion, so in large parts of bearing chamber, the droplet velocity is less affected by air pressure. However, the reason for the velocity of droplet, which is close to the chamber wall and is decreased with the increasing air pressure, is that: the region in the vicinity of chamber wall ($r \geqslant$ 150 mm) is close to vent too, the inlet airflow mass rate is increased with increasing air pressure, and the outlet airflow mass rate and velocity are increased consequently, then the drag force from airflow to droplet is increased and the velocity of droplet is decreased lastly.

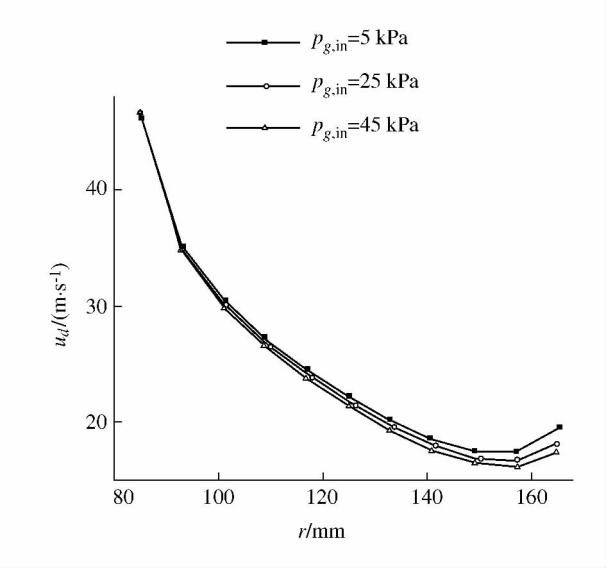

Figure 4 Effect of sealing air pressure on oil droplet velocity

Figure 5 shows the effect of sealing air pressure on oil droplet trajectory, whose diameter is 80 μm. Closing to the chamber wall ($r \geqslant 150$ mm), with the increasing air pressure, the migration of droplet trajectory is decreased in tangential direction while increased in axial direction. The reasons are that: with increasing air pressure, the tangential velocity of airflow is decreased and then the drag force applied to droplet in tangential direction is decreased, the migration of droplet trajectory in tangential direction is decreased; however, the axial velocity of airflow is increased near vent and then the drag force applied to droplet in axial direction is increased, the migration of droplet trajectory in axial direction is increased.

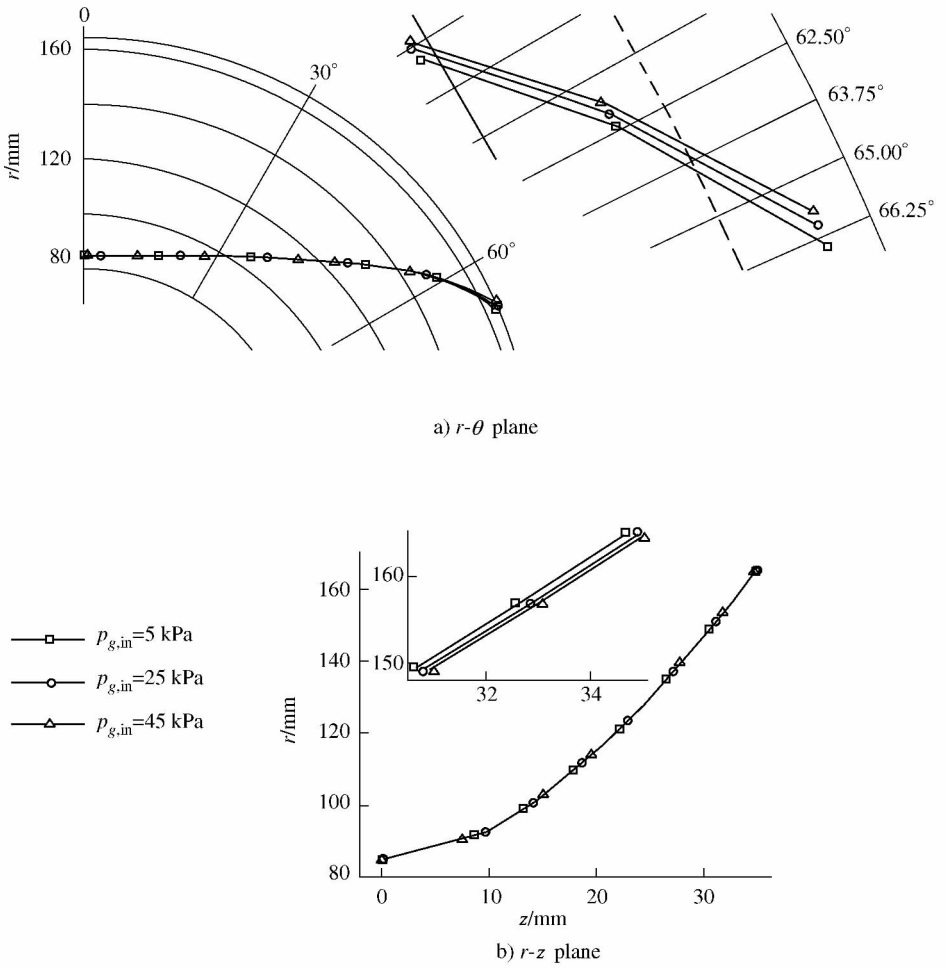

Figure 5 Effect of sealing air pressure on oil droplet trajectory

5.2 Influence on oil film thickness and velocity

The thickness and average velocity of oil film in bearing chamber are calculated under low and high rotational rates (n_s =6 500 r/min and n_s =14 500 r/min) respectively, Figure 6 shows the effect of sealing air pressure on oil film thickness and average velocity. With the exception of the effect of sealing air pressure on oil film thickness is significant under high rotational rates; the values of oil film thickness and average velocity are insensitive to variation of sealing air pressure under other conditions. The reasons are that: on one hand, the sealing air pressure has unapparent impact on deposition mass and momentum of droplet/wall impingement, on the other hand, although considering the effect of sealing air pressure on air/wall shear force, the deposition mass and momentum play leading roles in the oil film motion comparing to air/wall shear force, so the oil film thickness and average velocity show little sensitivity to sealing air pressure. However, under high rotational rates, the reason for the oil film thickness is increased with increasing air pressure in the down side of chamber ($\theta > 180°$) is that the first deposited mass is increased with increasing pressure. In the rising side of chamber ($\theta < 180°$) , the air/film shear has in the opposite direction of gravity and the film is found to hang on the wall of this side, the change of film is instability consequently.

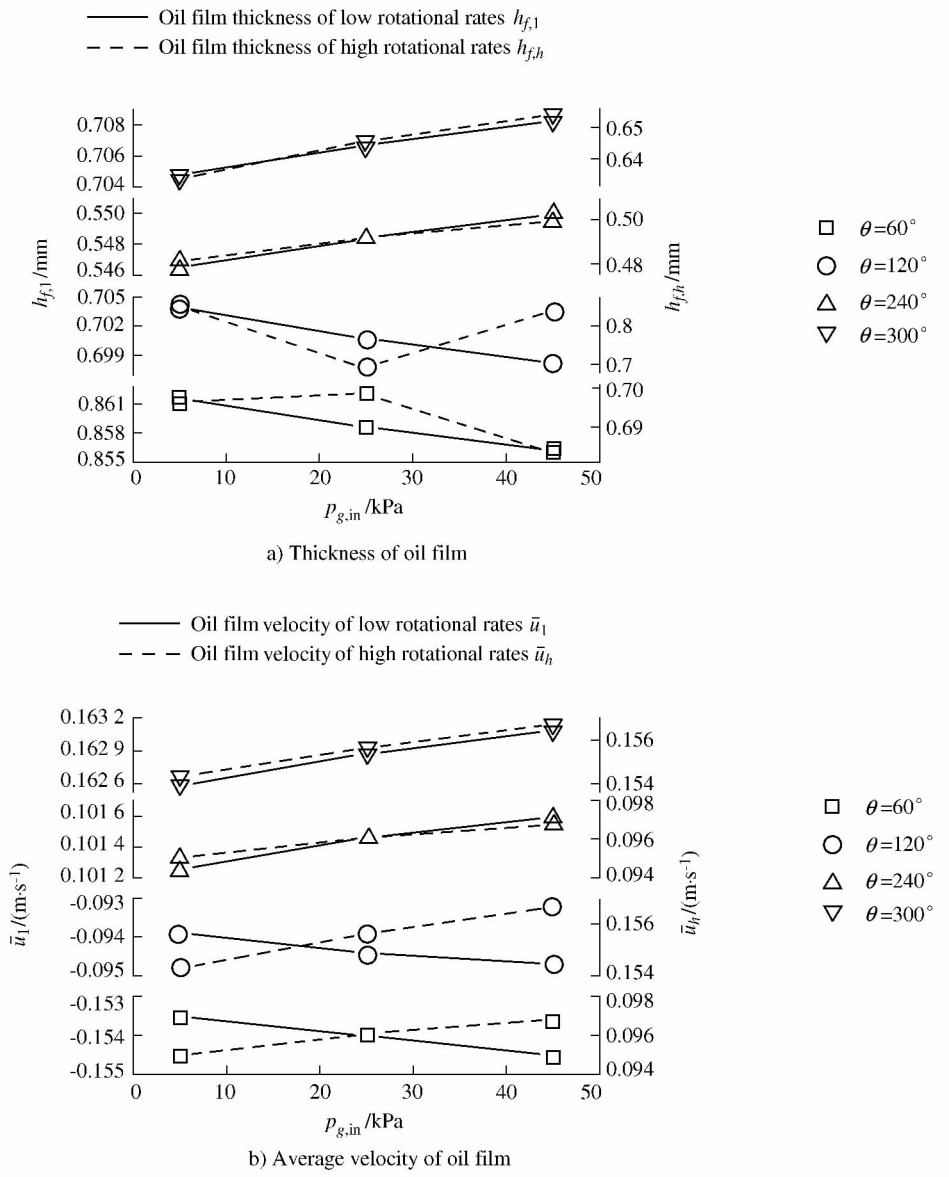

Figure 6 Effect of sealing air pressure on oil film thickness and velocity

6 Conclusions

1) The airflow tangential velocity and air/wall shear force in bearing chamber are decreased with increasing sealing air pressure.

2) With increasing sealing air pressure, near the chamber wall, the oil droplet velocity and motion migration in tangential direction are decreased while the motion migration in axial direction are increased; far away from the chamber wall, the oil droplet velocity and trajectory show little sensitivity to air pressure.

3) Under high rotational rate, the oil film thickness is increased with increasing air pressure in the down side of chamber while the oil film velocity, as well as oil film velocity and thickness under low rotational rate are insensitive to air pressure.

References

[1] Lee C W, Palma P C, Simmons K, Pickering S J. Comparison of computational fluid dynamics and particle image velocimetry data for the airflow in an aeroengine bearing chamber [J]. ASME, Journal of Engineering for Gas Turbines and Power, 2005, 127(4): 697 ~ 703

[2] Glahn A, Kurreck M, Willmann M, Wittig S. Feasibility study on oil droplet flow investigations inside aero engine bearing chambers-PDPA techniques in combination with numerical approaches [J]. ASME, Journal of Engineering for Gas Turbines and Power, 1996, 118(4): 749 ~ 755

[3] Gorse P, Busam S, Dullenkopf K. Influence of operating condition and geometry on the oil film thickness in aeroengine bearing chambers [J]. ASME, Journal of Engineering for Gas Turbines and Power, 2006, 128(1): 103 ~ 110

[4] Farrall M, Hibberd S, Simmons K. The effect of initial injection conditions on the oil droplet motion in a simplified bearing chamber [J]. ASME, Journal of Engineering for Gas Turbines and Power, 2008, 130(1): 12501 ~ 12507

[5] Wang J, Chen G D, Liu Y J. The analysis of airflow in the chamber-rotating structure [J]. Machinery Design & Manufacture, 2010, (10): 192 ~ 194 (In Chinese)

[6] Chen B, Chen G D, Zhang Y H, Sun H C. Numerically simulating airflow field inside aeroengine bearing chamber [J]. Mechanical Science and Technology for Aerospace Engineering, 2012, 31(8): 1241 ~ 1246 (In Chinese)

[7] Wang J, Chen G D, Liu Y J. Analysis of the oil droplet motion and deposition characteristics in an aeroengine bearing chamber [J]. Tribology, 2010, 30, (4): 361 ~ 366 (In Chinese)

[8] Chen G D, Chen B, Wang J, Chen C. Oil droplet size distribution and deposition properties in bearing chamber [J]. Journal of Mechanical Engineering, 2011, 47(10): 139 ~ 144 (In Chinese)

[9] Chen G D, Sun H C, Wang J. Research into configuration and flow of wall oil film in bearing chamber based on droplet size distribution [J]. Chinese Journal of Aeronautics, 2011, 24(3): 355 ~ 362

[10] Ishii M, Hibiki T. Thermo-fluid Dynamics of Two-phase Flow [M]. New York: Springer, 2006: 309 ~ 314

[11] Farrall M, Hibberd S, Simmons K, Giddings D. Prediction of air/oil exit flows in a commercial aero-engine bearing chamber [J]. Journal of Aerospace Engineering, 2006, 220(3): 197 ~ 202

Brief Biographies

SUN Heng-chao is a Ph. D candidate in School of Mechanical Engineering of Northwestern Polytechnical University. His research interest is lubrication design of aeroengine. shc361@163.com.

CHEN Guo-ding is a professor of Northwestern Polytechnical University. His main research interests include tribology and mechanical design. gdchen@nwpu.edu.cn.

YOU Hao is a master degree candidate in School of Mechanical Engineering of Northwestern Polytechnical University. His research interest is lubrication design of aeroengine.

CHEN Jun-yu is a master degree candidate in School of Mechanical Engineering of Northwestern Polytechnical University. His research interest is lubrication design of aeroengine.